Computer Physics Communications xxx (xxxx) xxx

Contents lists available at ScienceDirect

Computer Physics Communications

journal homepage: www.elsevier.com/locate/cpc

Solving the Grad–Shafranov equation using spectral elements for tokamak equilibrium with toroidal rotation☆

Haolong Li [a], Ping Zhu [b,c,*]

[a] CAS Key Laboratory of Geospace Environment and Department of Engineering and Applied Physics, University of Science and Technology of China, Hefei, Anhui 230026, China

[b] International Joint Research Laboratory of Magnetic Confinement Fusion and Plasma Physics, State Key Laboratory of Advanced Electromagnetic Engineering and Technology, School of Electrical and Electronic Engineering, Huazhong University of Science and Technology, Wuhan, Hubei 430074, China

[c] Department of Engineering Physics, University of Wisconsin-Madison, Madison, WI 53706, USA

ARTICLE INFO

Article history:
Received 9 June 2019
Received in revised form 29 November 2019
Accepted 9 March 2020
Available online xxxx

Keywords:
Magnetohydrodynamic equilibrium
Grad–Shafranov equation
NIMEQ
NIMROD
Toroidal rotation
Tokamak

ABSTRACT

The Grad–Shafranov equation is solved using spectral elements for tokamak equilibrium with toroidal rotation. The Grad–Shafranov solver builds upon and extends the NIMEQ code (Howell and Sovinec, 2014) previously developed for static tokamak equilibria. Both geometric and algebraic convergence are achieved as the polynomial degree of the spectral-element basis increases. A new analytical solution to the Grad–Shafranov equation is obtained for Solov'ev equilibrium in presence of rigid toroidal rotation, in addition to a previously obtained analytical solution for a different set of equilibrium and rotation profiles. The numerical solutions from the extended NIMEQ are benchmarked with the analytical solutions, with good agreements. Besides, the extended NIMEQ code is benchmarked with the FLOW code (Guazzotto et al., 2004). The modification of pressure profile induced by toroidal flow is investigated. The relative change of pressure profile is found significant around the edge.

1. Introduction

For the static equilibrium, the magnetohydrodynamic (MHD) equations yield nonlinear second order differential equation known as Grad–Shafranov equation [1,2]. The steady state equilibria defined by the solutions of Grad–Shafranov (GS) [1,2] equation act as the foundation for evaluating the MHD stability of tokamak plasma. Numerical codes have been developed based on different algorithms to solve nonlinear GS equation for given plasma density, temperature and magnetic field profiles directly from experiment [3,4]. However, most of these codes have only considered the static tokamak equilibrium where plasma flow such as the toroidal rotation is absent.

Toroidal rotation plays significant roles in many tokamak plasma processes. For example, plasma flow and flow shear above a certain threshold may lead to the formations of H-mode and internal transport barrier (ITB) [5–7]. Meanwhile, plasma flow and flow shear can also directly affect plasma stability and transport [8–13]. In particular, flow shear may have stabilizing effects on neoclassical tearing modes(NTMs) [14,15], tearing modes (TMs) [16–19] and edge localized modes (ELMs) [12,20–22]. It is found that sufficient toroidal flow opens up a stability window for resistive wall mode (RWM) [11,23–26]. On the other hand, plasma flow and shear can also directly modify plasma equilibrium due to the centrifugal effect.

There is a rich history of analytic solutions to the GS equation [27–34]. For example, the solution of the GS homogeneous equation is given by S. B. Zheng [27]. The inhomogeneous GS equation with linear source functions P and F known as Solov′ev equilibrium can be solved analytically for any two parameters [27,28,35]. The solution to the GS equation with parabolic source functions has been also reported, which allow independent specifications of plasma current density, pressure ratio and one shape moment such as the internal inductance [30,31]. Meanwhile, the analytical solution to the vacuum Grad–Shafranov equation has been worked out in cap-cyclide coordinates [36]. Besides tokamak, equilibria of other configurations also have been obtained analytically, such as those of the field-reversed configuration (FRC) [32,33].

However, the equilibria that can be described using analytic solutions of GS equation are limited. GS equation often has to be solved numerically, based on the choice of either the flux along the boundary or the source functions. Fixed-boundary solvers specify the flux value along the boundary of

☆ The review of this paper was arranged by Prof. David W. Walker.

* Corresponding author at: International Joint Research Laboratory of Magnetic Confinement Fusion and Plasma Physics, State Key Laboratory of Advanced Electromagnetic Engineering and Technology, School of Electrical and Electronic Engineering, Huazhong University of Science and Technology, Wuhan, Hubei 430074, China.

E-mail address: zhup@hust.edu.cn (P. Zhu).

https://doi.org/10.1016/j.cpc.2020.107264
0010-4655/

the computation domain. Free-boundary solvers self-consistently calculate the flux value along the boundary of computation, combining the contribution from external magnetic coils and the contribution from internal plasma current. Various numerical methods have been applied to solving the GS equation, for example, finite difference [37], spectral methods [38], Green's functions [39], linear finite elements [40,41], and Hermite cubic finite elements [42]. Consequently, many numerical toroidal equilibrium codes have been developed, such as EFIT [4], CHEASE [3], ESC [43], NIMEQ [44], etc.

In addition, several codes are able to solve for toroidal equilibrium in presence of flow, such as FLOW [8], CLIO [45] and FINESSE [46]. But these codes are often designed for topologically toroidal domains and do not consider the regularity issues associated with the R^{-1} singularity, where R is the major radius. This issue would arise in topologically cylindrical domains, which include the geometric axis $R = 0$. Previously, a Grad–Shafranov solver NIMEQ [44] was developed for static toroidal equilibrium within the framework of NIMROD [47]. In topologically cylindrical domains, regularity requires the flux function to vary as $\psi(R, Z) \approx \psi_0 + \psi_2(Z)R^2$ in the limit of $R \to 0$, where ψ_0 is constant, and ψ_2 is an unspecified function of Z. NIMEQ imposes the regularity condition, thus allows solutions on topologically cylindrical domains including the location where $R = 0$.

In this work, we extend the Grad–Shafranov solver NIMEQ [44] to solution of the toroidal equilibrium in presence of toroidal rotation. A new analytical solution of the modified Grad–Shafranov equation is found. The extended NIMEQ is benchmarked with the new analytical solution and the analytical solution by Maschke and Perrin [48]. The convergence of the extended NIMEQ is tested with h-refinement and p-refinement methods. Furthermore, the extended NIMEQ is benchmarked with FLOW in a convergence study. Due to the significant role of toroidal rotation and the wide applications of the NIMROD code, it is worthwhile to extend the GS solver companion of NIMROD code–NIMEQ to include effects of toroidal rotation on the equilibrium. Such an effort may deserve a detailed and formal documentation in this paper, which includes not only a description of the formulation and algorithm, but also a report on the benchmark between the extended NIMEQ and analytical solutions as well as the FLOW code. Another finding worth mentioning is the identification of the optional value of the relaxation parameter θ in Eq. (23), which is not necessarily same as and turns out indeed different from the one in absence of toroidal rotation.

The rest of this paper is organized as follows. Section 2 reviews the Grad–Shafranov equation with toroidal rotation. Section 3 shows a new analytical solution to the modified Grad–Shafranov equation along with the analytical solution obtained by Maschke and Perrin [48]. Section 4 presents the numerical algorithm of the extended NIMEQ. Benchmarking and convergence studies are performed with these two equilibria in section 5. In section 6, the modification of pressure profile induced by toroidal flow is investigated for L-mode and H-mode equilibria. Finally, section 7 gives a conclusion and discussion.

2. Grad–Shafranov equation with toroidal rotation

Tokamak equilibria with toroidal rotation are governed by four equations: the force balance equation, magnetic divergence constraint, Ampere's law and state equation of ideal gas [49,50]

$$\rho(\vec{u}\cdot\nabla)\vec{u} = -\nabla P + \vec{J}\times\vec{B} \tag{1}$$

$$\nabla\cdot\vec{B} = 0 \tag{2}$$

$$\mu_0\vec{J} = \nabla\times\vec{B} \tag{3}$$

$$P = \frac{\rho}{m_i}T \tag{4}$$

where $\vec{u} = R^2\Omega\nabla\phi$ denotes the toroidal flow velocity, Ω the frequency of toroidal rotation, P the plasma pressure, $\vec{J}$ the plasma current density, $\vec{B}$ the magnetic field and μ_0 the permeability of vacuum. Besides, ρ denotes the mass density, defined as $\rho \equiv m_i n_i + m_e n_e \simeq m_i n$, $n \equiv n_i = n_e$ and T denotes the plasma temperature defined as $T \equiv T_i + T_e$, where $m_i(m_e)$, $n_i(n_e)$ and $T_i(T_e)$ are the ion (electron) mass, number density and temperature.

The magnetic field is expressed as $\vec{B} = \nabla\phi\times\nabla\psi + F\nabla\phi$ and the plasma current is expressed as $\mu_0\vec{J} = \mu_0 R J_\phi\nabla\phi + \nabla F\times\nabla\phi$ in the cylindrical coordinate system and $F(\psi) = RB_\phi$ is a flux function [44]. From the curl of Ohm's law, it is observed that the frequency of toroidal rotation is a flux function $\Omega = \Omega(\psi)$. Substituting these above expressions for $\vec{B}$, $\vec{J}$ and $\vec{u}$ into Eq. (1) yields:

$$\rho R\Omega^2 - \frac{\partial P}{\partial R} = 0 \tag{5}$$

$$\Delta^*\psi = -R^2\frac{\partial P}{\partial\psi} - F\frac{dF}{d\psi} \tag{6}$$

where the Grad–Shafranov operator is defined as

$$\Delta^* \equiv R\frac{\partial}{\partial R}R^{-1}\frac{\partial}{\partial R} + \frac{\partial^2}{\partial Z^2} \tag{7}$$

For fusion plasma the thermal conduction along magnetic field lines is fast compared to the heat transport perpendicular to a magnetic surface. Thus, plasma temperature can be considered as a flux function, namely $T = T(\psi)$. From Eq. (5), the pressure is integrated as:

$$P(\psi, R) = P_0(\psi)\exp\left[\frac{m_i\Omega^2R_0^2}{2T}\left(\frac{R^2}{R_0^2} - 1\right)\right] \tag{8}$$

Substituting $P(\psi, R)$ into Eq. (6), we have

$$\Delta^*\psi = -F\frac{dF}{d\psi} - \mu_0R^2\left[\frac{dP_0}{d\psi} - P_0\frac{m_iR_0^2\Omega}{T}(\frac{R^2}{R_0^2} - 1)\frac{d\Omega}{d\psi} + P_0\frac{m_iR_0^2\Omega^2}{2T^2}(\frac{R^2}{R_0^2} - 1)\frac{dT}{d\psi}\right]\exp\left[\frac{m_i\Omega^2R_0^2}{2T}\left(\frac{R^2}{R_0^2} - 1\right)\right] \tag{9}$$

where R_0 denotes the position of magnetic axis. $P = P_0(\psi)$ when $\Omega = 0$. In the limit $\Omega \to 0$, the static equilibrium pressure can be recovered as a flux function. Meanwhile, Eq. (9) will reduce to the static GS equation.

3. Analytical solutions

3.1. Solov'ev equilibrium with toroidal rotation

We obtain a new analytical solution to Eq. (9) for Solov'ev equilibrium in presence of toroidal rotation. In Solov'ev equilibrium, we assume that:

$$\mu_0P_0' = p_1 \tag{10}$$

$$FF' = F_0 \tag{11}$$

where p_1 and F_0 are constants [51]. Furthermore, the plasma temperature and frequency of toroidal rotation are assumed to be constants T_0 and Ω_0 respectively, i.e. $T = T_0$, $\Omega = \Omega_0$

The Grad–Shafranov equation Eq. (9) is reduced to

$$\Delta^*\psi = -p_1R^2\exp[M_0^2(\frac{R^2}{R_0^2} - 1)] - F_0 \tag{12}$$

where $M_0 = \frac{m_iR_0^2\Omega_0^2}{2T_0}$ denotes the Mach number at $R = R_0$.

The solution of Eq. (12) is of the form $\psi(R, Z) = \psi_p(R, Z) + \psi_h(R, Z)$, where ψ_p is the particular solution and ψ_h is the homogeneous solution [27,51].

$$\psi_h = c_1 + c_2R^2 + c_3(R^4 - 4R^2Z^2) + c_4[R^2ln(R) - Z^2] \tag{13}$$

Please cite this article as: H. Li and P. Zhu, Solving the Grad–Shafranov equation using spectral elements for tokamak equilibrium with toroidal rotation, Computer Physics Communications (2020) 107264, https://doi.org/10.1016/j.cpc.2020.107264.

where these constants c_1, c_2, c_3, c_4 are determined by boundary condition. Then, for a particular solution:

$$\psi_p = -p_1\left(\frac{R_0^2}{2M_0^2}\right)^2\left\{\exp\left[M_0^2\left(\frac{R^2}{R_0^2}-1\right)\right]-\frac{M_0^2}{R_0^2}\left(R^2-R_0^2\right)-1\right\} -\frac{F_0}{2}Z^2 \tag{14}$$

We obtain a new analytical solution of Grad–Shafranov equation for the Solov'ev equilibrium with toroidal rotation:

$$\begin{aligned}\psi &= \psi_p+\psi_h = c_1+c_2R^2+c_3(R^4-4R^2Z^2) \\ &+c_4[R^2ln(R)-Z^2] \\ &-p_1\left(\frac{R_0^2}{2M_0^2}\right)^2\left\{\exp\left[M_0^2\left(\frac{R^2}{R_0^2}-1\right)\right]-\frac{M_0^2}{R_0^2}\left(R^2-R_0^2\right)-1\right\} \\ &-\frac{F_0}{2}Z^2\end{aligned} \tag{15}$$

This solution reduces to the solution of static Solov'ev equilibrium when $\Omega_0 \to 0$ or $M_0 \to 0$.

$$\psi = \lim_{M_0\to 0}\psi_h+\psi_p = \psi_h+\lim_{M_0\to 0}\psi_p = \psi_h - p_1\frac{(R^2-R_0^2)^2}{8}-\frac{F_0}{2}Z^2 \tag{16}$$

The above solution in Eq. (16) was a specific case of the Grad–Shafranov equation solutions obtained before in Ref. [27]. A similar solution of Solov'ev equilibrium with rigid toroidal rotation was recently obtained by Chu et al. [52],

$$\begin{aligned}\psi &= \psi_h - p_1\left(\frac{R_0^2}{2M_0^2}\right)^2\left\{\exp\left[M_0^2\left(\frac{R^2}{R_0^2}-1\right)\right]\right. \\ &\left.-\frac{M_0^2}{R_0^2}\left(R^2-R_0^2\right)-1\right\}-\frac{F_0}{2}Z^2 \\ &+\frac{1-2\beta_{pJ}}{16}\left[(\frac{R^2}{R_0^2}-1)^2-\frac{4R^2Z^2}{R_0^4}\right]\end{aligned} \tag{17}$$

where $\beta_{pJ} = -\frac{R_0^2 p_1}{F_0+R_0^2 p_1}$. The two solutions in Eqs. (15) and (17) are equivalent, even though they are obtained independently. The apparent difference between Eqs. (15) and (17) comes from different specific choices of the coefficients c_1, c_2, c_3 and c_4 in the homogeneous solution ψ_h, which correspond to different boundary conditions. However, the particular solution ψ_p in Chu's analytical solution above in Eq. (17) contains some terms that actually belong to the homogeneous solution. In contrast, the particular solution and the homogeneous solution are clearly and completely separated in our solution in Eq. (15).

3.2. Maschke–Perrin equilibrium

Another analytic solution of Eq. (6) was previously found based on the following assumptions [48]:

$$P = \frac{P_0}{R_L^4}(\psi-\psi_1)\exp\left(\gamma R^2\Omega^2/2R_L^2\right) \tag{18}$$

$$F^2 = F_0^2+2\frac{M}{R_L^2}(\psi-\psi_1) \tag{19}$$

$$\frac{\omega^2}{RT} = \text{constant} = \gamma\frac{\Omega^2}{R_L^2} \tag{20}$$

where γ is the ratio of specific heats and R_L P_0, ψ_1, F_0, M, Ω are constants. Ω denotes the Mach number in Maschke–Perrin analytical solution. Different from the Solov'ev equilibrium with toroidal rotation, in the Mashke–Perrin equilibrium, the toroidal rotation is not a constant, instead the frequency of toroidal rotation $\omega^2 \propto T$ [Eq. (20)].

In case of $M = 0$, the analytical solution takes the form

$$\begin{aligned}\psi-\psi_1 &= CP_0\frac{R^2}{R_L^2} \\ &+P_0\left\{\frac{(\epsilon_a-1)}{4}\left(\frac{Z^2}{R_L^2}-\frac{R^2}{4R_L^2}\right)\frac{R^2}{R_L^2}\right. \\ &\left.+\frac{1}{\gamma^2\Omega^4}\left[1+\frac{\gamma\Omega^2R^2}{2R_L^2}-\exp\left(\frac{\gamma\Omega^2R^2}{2R_L^2}\right)\right]\right\}\end{aligned} \tag{21}$$

where $C = \frac{(\epsilon_a-1)}{8}r_a^2+\frac{1}{2\gamma\Omega^2}\left[\exp\left(\frac{\gamma\Omega^2r_a^2}{2}-1\right)\right]$ is a constant, ϵ_a is a constant related to the ellipticity of the plasma cross-section, $r_a = R_0/R_L$ denotes the ratio between the position of magnetic axis R_0 and the chosen scale length R_L.

4. Numerical algorithm

NIMEQ solves the Grad–Shafranov equation in weak form using Galerkin formulation [44]. Defining one scalar field $\Lambda = \psi/R^2$, the Grad–Shafranov operator can be transformed into a divergence of a vector, $\Delta^*\psi = \nabla\cdot R^2\nabla\Lambda$. The scalar field Λ can be spilt into two parts: Λ_0 and Λ_h where Λ_0 satisfies the specified inhomogeneous boundary condition for Λ and Λ_h satisfies the boundary condition $\Lambda_h = 0$. The Λ_h is expended onto a series of C^0 spectral element basis functions $\Lambda_h = \sum_i \Lambda_i\alpha_i$. The weak form of Grad–Shafranov equation is obtained as:

$$\begin{aligned}&\sum_i \Lambda_i\int dVR^2\nabla\alpha_i\cdot\nabla\alpha_j = \\ &\int dV\left\{FF'+\mu_0R^2\left[\frac{dP_0}{d\psi}+P_0\frac{m_iR_0^2\Omega}{T}\left(\frac{R^2}{R_0^2}-1\right)\frac{d\Omega}{d\psi}\right.\right. \\ &\left.-P_0\frac{m_iR_0^2\Omega^2}{2T^2}\left(\frac{R^2}{R_0^2}-1\right)\frac{dT}{d\psi}\right] \\ &\left.\exp\left[\frac{m_i\Omega^2R_0^2}{2T}\left(\frac{R^2}{R_0^2}-1\right)\right]\right\}\alpha_j-\int dVR^2\nabla\Lambda_0\cdot\nabla\alpha_j\end{aligned} \tag{22}$$

For compactness, Eq. (22) is written as $M\Lambda = Q$. The modified Picard iterations in Eq. (23), has been applied to solve the Grad–Shafranov equation in NIMEQ, where $\theta \in (0, 1]$ denotes the relaxation parameter to achieve convergence. The optimal range of relaxation parameter becomes smaller in rotating equilibrium compared with the static equilibrium.

$$M\Lambda^n = (1-\theta)M\Lambda^{n-1}+\theta Q^{n-1} \tag{23}$$

After iteration, these equilibrium fields are calculated from the converged solution for Λ. The pressure, temperature, toroidal flow velocity $\vec{u}_\phi$ and RB_ϕ values are calculated from the prescribed $P_0(\psi)$, $F(\psi)$, $T(\psi)$, $\Omega(\psi)$ using the converged solution $\Lambda(R, Z)$ through Eq. (8) and $\vec{u}_\phi = R^2\Omega(\psi)\nabla\phi$. The poloidal magnetic field is expressed as Eq. (24) in terms of Λ.

$$\vec{B}_p = \frac{1}{R}\hat{e}_\phi\times(2R\hat{e}_R\Lambda+R^2\nabla\Lambda) \tag{24}$$

where $\hat{e}_R$ and $\hat{e}_\phi$ represent the unit vectors in the R and ϕ directions respectively.

The poloidal current is calculated directly from the magnetic field through the relation $\vec{J}_p = -F'\vec{B}_p/\mu_0$. And the toroidal current density is calculated using Eq. (25)

$$J_\phi = \frac{1}{\mu_0 R}\Delta^*\psi = R\frac{\partial P}{\partial\psi}+\frac{1}{\mu_0 R}F\frac{\mathrm{d}F}{\mathrm{d}\psi} \tag{25}$$

Please cite this article as: H. Li and P. Zhu, Solving the Grad–Shafranov equation using spectral elements for tokamak equilibrium with toroidal rotation, Computer Physics Communications (2020) 107264, https://doi.org/10.1016/j.cpc.2020.107264.

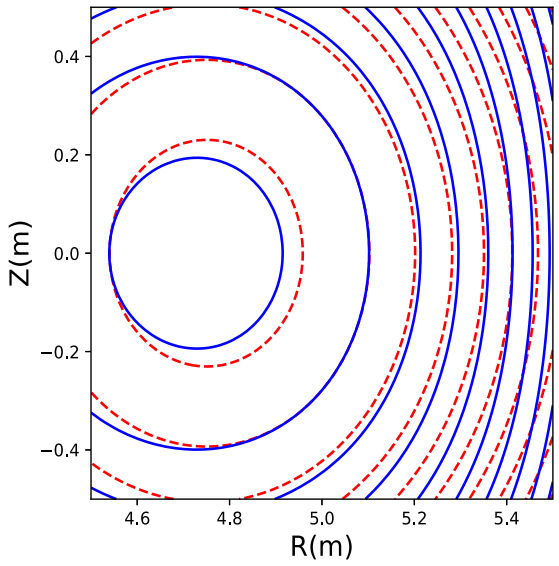

Fig. 1. The poloidal flux contour of the Solov'ev equilibrium with $p_1 = -8.0 \times 10^{-2}$, $F_0 = -20$ and $M_0 = 4$. The red dashed lines stand for the equilibrium without toroidal rotation. The blue solid lines stand for the equilibrium with toroidal rotation.

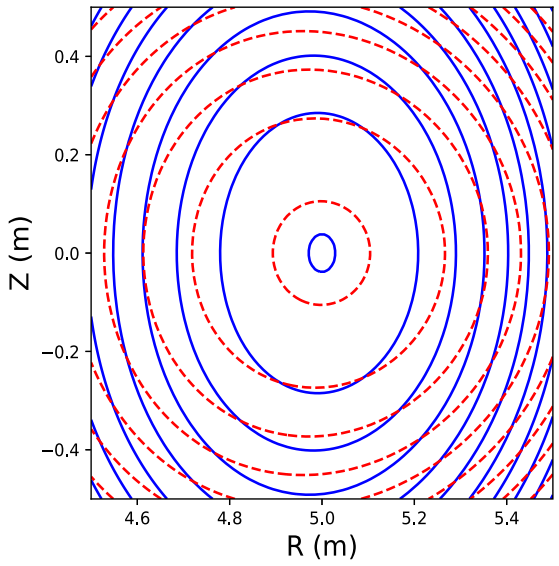

Fig. 2. The poloidal flux contour of the Maschke and Perrin's equilibrium with $P_0 = -8.0 \times 10^{-3} \times R_L^4$ and $\Omega = 5.0 \times 10^4$. The red dashed lines stand for the equilibrium without toroidal rotation. The blue solid lines stand for the equilibrium with toroidal rotation.

5. Benchmark and convergence

The analytic solutions in Section 3.1 are plotted in a domain of rectangular poloidal cross section with $4.5 < R < 5.5$ and $-0.5 < Z < 0.5$ (Fig. 1). Parameters are set as $p_1 = -0.176$, $F_0 = 0.5$, $M_0 = 0.3$ and the poloidal flux along the boundary is prescribed using Eq. (15), with $c_1 = 0.09390925$, $c_2 = 0.09390925$, $c_3 = -0.00264707$ and $c_4 = 0.13955081$. The values of rotation parameter chosen in these cases is around the Mach number of experimental estimates. In particular, the local peak values of Mach numbers in Section 6 correspond to those typically observed in L-mode and H-mode experiments. The equilibrium poloidal flux contours for Solov'ev equilibrium with toroidal rotation and without toroidal rotation presented in Fig. 1 show modification induced by toroidal rotation.

Similarly, the equilibrium poloidal flux contours for Maschke and Perrin's equilibrium in Section 3.2 are plotted in a domain of rectangular poloidal cross section with $4.5 \le R \le 5.5$ and $-0.5 \le Z \le 0.5$ (Fig. 2). In this case, we choose $\epsilon_a = 0$, $\gamma = 5/3$, $R_0 = R_L = 5.0$, $P_0 = -0.1 \times R_L^4$, $\Omega = 0.389$, $\psi_0 = 0$ and $\varepsilon_a = 0$. Distortion of flux surfaces due to toroidal rotation is also apparent.

Both benchmark and convergence studies are performed for Solov'ev equilibrium and Maschke and Perrin's equilibrium by comparing the numerical and analytical solutions. The numerical error of equilibrium poloidal flux is defined as $E_n = \sqrt{\sum(\psi_n - \psi_a)^2 / \sum \psi_a^2}$, where ψ_n is the numerical solution from the extended NIMEQ and ψ_a is the analytic solution from Eqs. (15) and (21). And the summation is performed over all of the finite-element nodes.

Two methods, i.e. h-refinement and p-refinement, are applied to checking the convergence of the extended NIMEQ in both equilibria. In the p-refinement method, the polynomial degree of each element is increased whereas the number of elements is kept constant. H-refinement maintains the polynomial degree of the elements while increasing the number of elements. The decaying rate of the error for a smooth solution of a second order differential equation is bounded by the asymptotic rate of convergence $h^{(p+1)}$ for sufficiently smooth solutions, where h is a characteristic element length of calculation region and p is the polynomial degree [53]. For the tokamak poloidal plane, the shape of finite element is often curved instead of straight-line rectangular. The same finite element mesh in NIMEQ are also meant to be used in NIMROD simulations, where the realistic thermal conduction is highly anisotropic. Previous study demonstrates that the high-order spectral element is necessary to achieve the desired accuracy and convergence under these circumstances [47].

We use meshes with equal numbers of elements in the radial and vertical directions. In the p-refinement study, the polynomial degree of elements is scanned from 2 to 10 when keeping the 2×2 and 8×8 element meshes fixed for Solov'ev equilibrium with toroidal flow and the polynomial degree of elements is scanned from 2 to 15 when keeping the 2×2 and 10×10 element meshes fixed for Maschke–Perrin equilibrium. In both equilibrium cases, the numerical errors decay linearly to a minimum value, which indicates geometric convergence in Figs. 3 and 5 [53]. The numerical error in 10×10 and 8×8 element meshes decays faster than that in 2×2 element meshes in both equilibria.

In h-refinement study, the number of elements are scanned from 4 to 94 when polynomial degree of elements keeps at 2 and 3 for Solov'ev equilibrium with toroidal flow and 2 and 4 for Maschke–Perrin equilibrium. In h-refinement studies of both equilibrium cases, the numerical errors decay linearly to a minimum value, indicating algebraic convergence in Figs. 4 and 6 [53]. The decay rate of numerical error with polynomial degree fixed at 3 and 4 is larger than that with polynomial degree fixed 2. These blue and red lines in both figures stand for the scaling fitted from the decaying numerical errors, where N denotes the number of elements. Both figures show that the decay rates of numerical error in ψ are between $p + 1$ and $p + 2$. The numerical error E_n in the case of the 4th order elements goes up slightly when the number of elements increases above the converged value in Figs. 4 and 6. The remanent and slightly going-up error is likely caused by the numerical errors associated with the numerical values of the coefficients c_1 to c_4 in the homogeneous part of the analytical solution ψ_h itself, because the numerical values of the

Please cite this article as: H. Li and P. Zhu, Solving the Grad–Shafranov equation using spectral elements for tokamak equilibrium with toroidal rotation, Computer Physics Communications (2020) 107264, https://doi.org/10.1016/j.cpc.2020.107264.

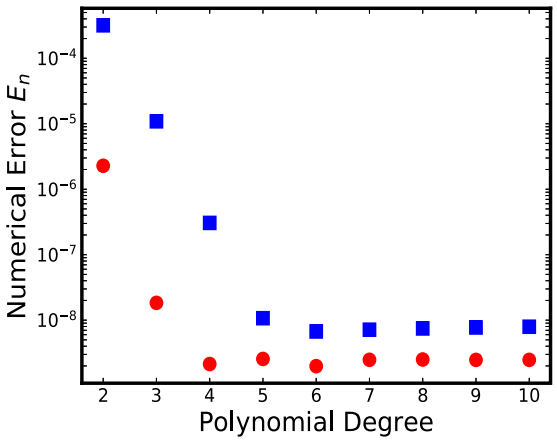

Fig. 3. The numerical error E_n of ψ as a function of the element polynomial degree for 2×2 element mesh (■) and 8×8 element mesh (●) in the case of Solov'ev equilibrium with toroidal rotation.

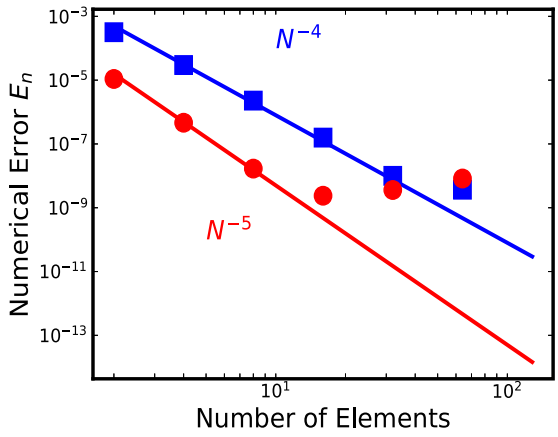

Fig. 4. The numerical error E_n of ψ as a function of the element numbers for 2nd order elements (■) and 3rd order elements (●) in the case of the Solov'ev equilibrium with toroidal rotation.

coefficients c_1 to c_4 are obtained numerically and approximately. This is a known issue with NIMEQ even without flow [44].

FLOW is a finite difference code, which solves the Bernoulli–Grad–Shafranov equations for tokamak the equilibria with flow [8]. The extended NIMEQ is benchmarked with the FLOW code here. The comparison is performed in a poloidal domain of $2.0 \leq R \leq 4$ and $-1.0 \leq Z \leq 1.0$. The F and Ω are chosen as constants. And the pressure profile is specified as one quadratic function of the normalized ψ, $P_0(\psi) = P_{\text{open}} + P_1(1-\psi) + 4P_2\psi(\psi-1)$. The number density profile is similar to the pressure profile, since $n(\psi) = \frac{P_0(\psi)}{P_0(0)} n_{\text{axis}}$, where $P_0(0)$ and n_{axis} denote the pressure and number density on magnetic axis. This number density profile is thus chosen so as to obtain a constant temperature. The Mach number is constant and equals 0.3. Since the solutions of the two codes are based on different methods of grid discretization, the number of grid points in FLOW is kept fixed at the converged value, and the number of grid points in NIMEQ is varied for comparison. The overlay of ψ forms the extended NIMEQ and FLOW is shown in Fig. 7. For comparison, the relatively numerical error is defined as $\sqrt{\sum(\psi_{\text{FLOW}} - \psi_{\text{NIMEQ}})^2 / \sum \psi^2_{\text{NIMEQ}}}$ where ψ_{NIMEQ} denotes the numerical solution from NIMEQ and ψ_{FLOW} denotes the numerical solution from FLOW. Because the computation grids are different in NIMEQ and FLOW, the bi-cubic spline interpolation is applied to calculation of relatively numerical error. The relative numerical error decreases with the computation grid point number (Fig. 8).

6. Toroidal rotation effects on equilibrium pressure profiles

In general, toroidal flow enhances (reduces) the equilibrium pressure in the low (high) field side. This can be seen from Eq. (8), which yields $P > P_0$ where $R > R_0$ and $P < P_0$ where $R < R_0$. To further quantify the influence on equilibrium pressure by toroidal flow, we apply the extended NIMEQ to solving the equilibrium pressure profile in presence of a rigid toroidal rotation for both an L- and an H-mode equilibrium. To proceed, we define the normalized magnetic flux $\psi \equiv (\psi - \psi_a/(\psi_l - \psi_a))$, where ψ_a and ψ_l are the flux on the magnetic axis and the last closed flux surface, respectively. Meanwhile, the relative change of pressure is defined as $\Xi = (P - P_0)/(P_0)$ to measure the effects induced by toroidal flow.

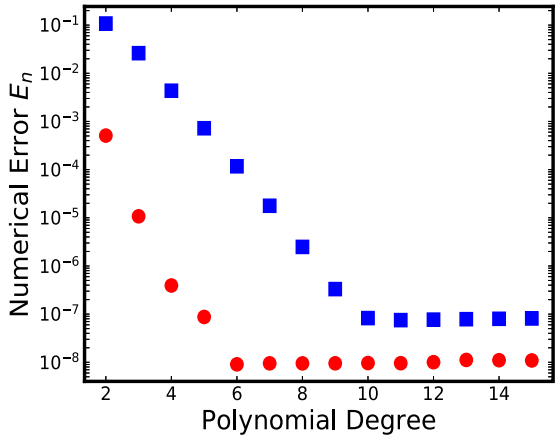

Fig. 5. The numerical error E_n of ψ as a function of the element polynomial degree for 2×2 element mesh (■) and 10×10 element mesh (●) in the case of Maschke and Perrin's equilibrium.

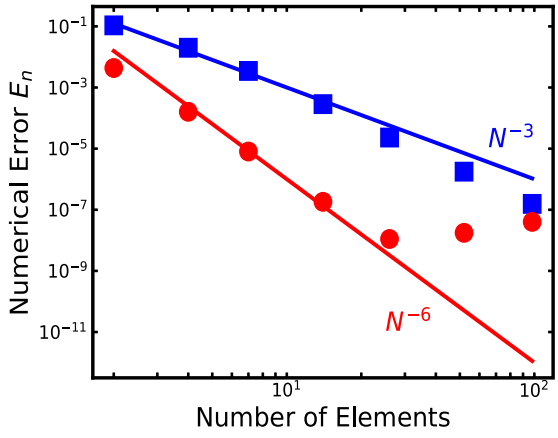

Fig. 6. The numerical error E_n of ψ as a function of the element numbers for 2nd order elements (■) and 4th order elements (●) in the case of Maschke and Perrin's equilibrium.

6.1. L-mode equilibrium

The static equilibrium for L-mode is based on the circular cross-section shown in Fig. 9 and the equilibrium profiles in Fig. 10. NIMEQ solutions indicate that the rigid rotation indeed

Please cite this article as: H. Li and P. Zhu, Solving the Grad–Shafranov equation using spectral elements for tokamak equilibrium with toroidal rotation, Computer Physics Communications (2020) 107264, https://doi.org/10.1016/j.cpc.2020.107264.

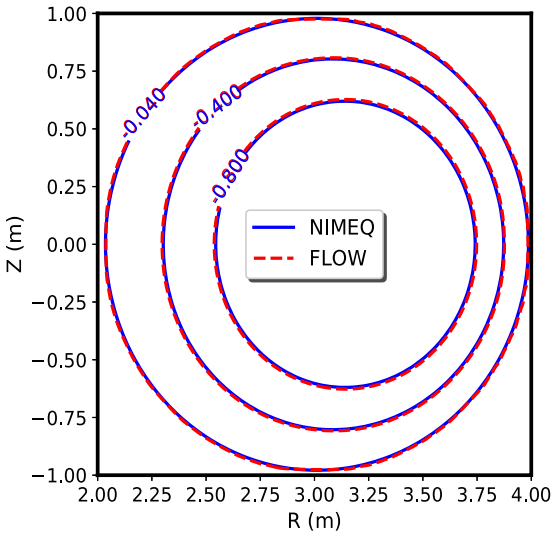

Fig. 7. The comparison between ψ from the extended NIMEQ and ψ from FLOW code, with $P_{\text{open}} = 1.0 \times 10^{-3}$, $P_1 = 0.8$, $P_2 = 0.2$, $n_{\text{axis}} = 8.0 \times 10^{19}$ and $F = 4.0$. The red dashed lines stand for the ψ from FLOW code and blue solid lines denote the ψ from the extended NIMEQ.

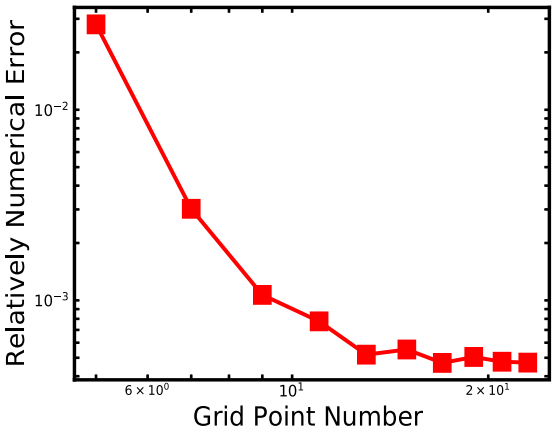

Fig. 8. The relatively error as a function of grid point number.

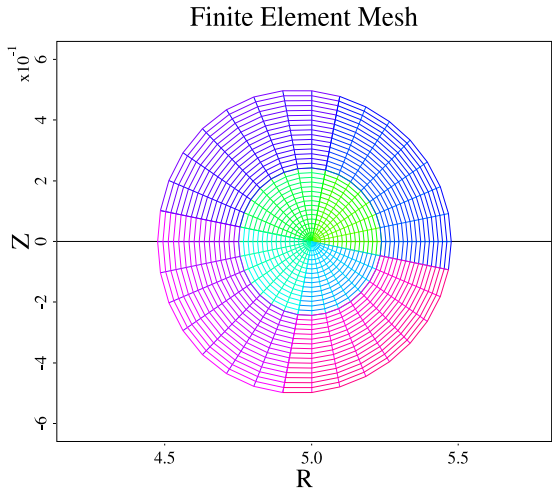

Fig. 9. The finite element mesh of poloidal plane with a circular cross-section for the L-mode and H-mode equilibria used in NIMEQ. The major radius $R_0 = 5.0$ m and the minor radius $a = 0.5$ m.

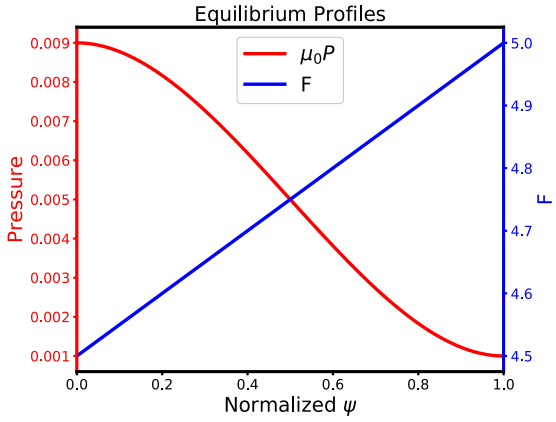

Fig. 10. L mode equilibrium pressure profile (red) and F profile (blue) as functions of the normalized ψ. (For interpretation of the references to color in this figure legend, the reader is referred to the web version of this article.)

makes Ξ negative in the high field side and positive in the low field side (Fig. 11). Namely, the rigid rotation makes pressure smaller in the high field side and larger in the low field side. The relative change of pressure profile increases with rigid rotation. The relative change in pressure profile induced by toroidal rotation is weak in the core region but significant in the edge region ($\leq$ 20%). The toroidal flow also generates a shift in flux surface along the $\vec{R}$ direction. In the midplane, the shift is measured by $\frac{R_\Omega - R_s}{a}$, where the R_Ω denotes the major radius of a particular poloidal flux surface in presence of toroidal flow, R_s denotes the major radius of the same flux surface in static equilibrium, and a denotes the minor radius. It is found that the shift of flux surface is a linear function of the square of Mach number (Fig. 12). The slope of the flux shift is lower for the flux surface closer to the edge region.

6.2. H-mode equilibrium

The grid of the static equilibrium for H-mode is same as the L-mode equilibrium in Fig. 9, and the H-mode equilibrium profiles are shown in Fig. 13. There is an edge pedestal in pressure profile, the form $P_0 = \frac{1}{2} p_0 \{\tanh[S(\psi_{pd} - \psi)] + 1\}$ where ψ_{pd} denotes the pedestal position and S represents the gradient of pedestal. In these cases, a uniform temperature profile is applied to avoid singular Mach number near the pedestal foot region. The maximum relative change of pressure is similar to that in L-mode, however, such a significant change of pressure is only narrowly localized in the pedestal region in H-mode (Fig. 14).

7. Conclusion and discussion

We have extended NIMEQ by solving the modified Grad–Shafranov equation that self-consistently takes into account of the effects of toroidal rotation. A new analytic solution to the modified Grad–Shafranov equation is obtained for the Solov'ev equilibrium in presence of a rigid toroidal rotation. Both the new analytical solution and the Maschke–Perrin equilibrium are used in benchmark and convergence studies. High accuracy solution with numerical error to the order of 10^{-10} or smaller is achieved. The extended NIMEQ is also successfully benchmarked with the FLOW code.

Please cite this article as: H. Li and P. Zhu, Solving the Grad–Shafranov equation using spectral elements for tokamak equilibrium with toroidal rotation, Computer Physics Communications (2020) 107264, https://doi.org/10.1016/j.cpc.2020.107264.

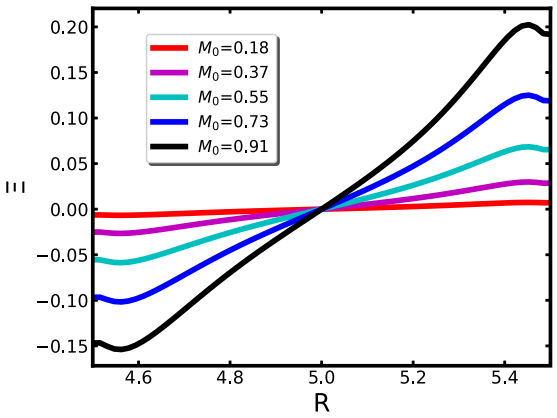

Fig. 11. The relative change of pressure as a function of R for different Mach number M_0 at the magnetic axis ($M_0 = \frac{m_i R_0^2 \Omega^2}{2T}$) in the L-mode case.

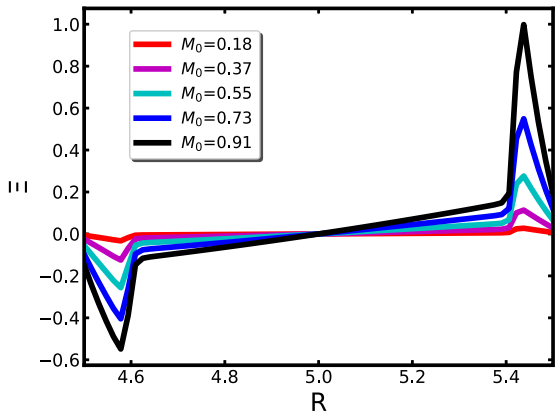

Fig. 14. The relative change of pressure as a function of R for different Mach number M_0 at the magnetic axis ($M_0 = \frac{m_i R_0^2 \Omega^2}{2T}$) in the H-mode case.

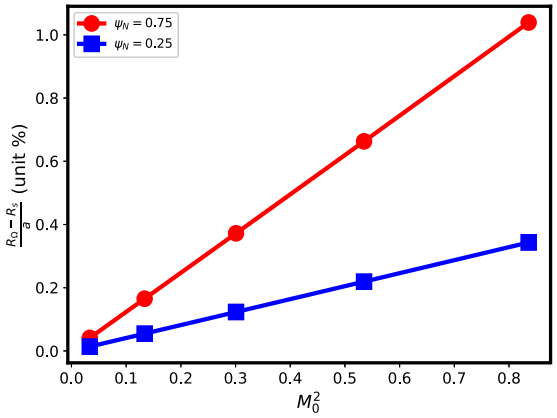

Fig. 12. The shift of flux surface measured by $\frac{R_\Omega - R_s}{a}$ as a function of the square of the Mach number at magnetic axis for two different magnetic flux surfaces.

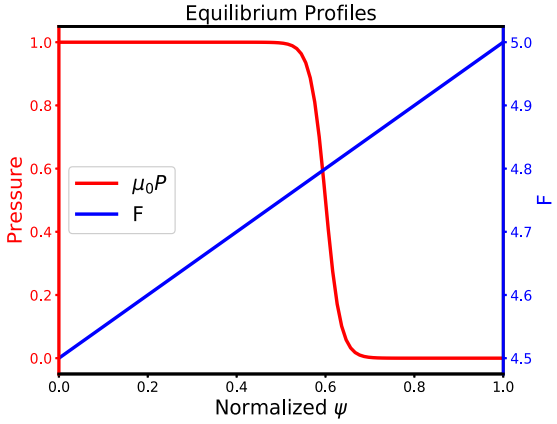

Fig. 13. H mode equilibrium pressure profile (red) and F profile (blue) as functions of the normalized ψ. (For interpretation of the references to color in this figure legend, the reader is referred to the web version of this article.)

The extended NIMEQ is applied to studying the effect of toroidal flow on both an L- and an H-mode. Toroidal flow makes equilibrium pressure smaller in the high field side and larger in the low field side. The relative change in pressure profile induced by toroidal rotation is weak in the core region but significant in the edge region ($\leq$ 20%). The flux shift due to toroidal flow is stronger in the core region than in the edge region.

Next, we plan to extend the modified Grad–Shafranov equation to include free boundary condition and poloidal flow.

Declaration of competing interest

The authors declare that they have no known competing financial interests or personal relationships that could have appeared to influence the work reported in this paper.

Acknowledgments

We are grateful for the support from the NIMROD team. This work was supported by the Fundamental Research Funds for the Central Universities at Huazhong University of Science and Technology Grant No. 2019kfyXJJS193, the National Natural Science Foundation of China Grant Nos. 11775221 and 51821005, and U.S. Department of Energy Grant Nos. DE-FG02-86ER53218 and DE-SC0018001. This research used the computing resources from the Supercomputing Center of University of Science and Technology of China.

References

[1] H. Grad, H. Rubin, J. Nucl. Energy 7 (3–4) (1958) 284–285, (1954).
[2] V.D. Shafranov, Sov. Phys. JETP 6 (3) (1958) 1013.
[3] H. Lütjens, A. Bondeson, O. Sauter, Comput. Phys. Commun. 97 (3) (1996) 219–260.
[4] L.L. Lao, H.E. St. John, Q. Peng, J.R. Ferron, E.J. Strait, T.S. Taylor, W.H. Meyer, C. Zhang, K.I. You, Fusion Sci. Technol. 48 (2) (2005) 968–977.
[5] S. Ding, A.M. Garofalo, J. Qian, L. Cui, J.T. McClenaghan, C. Pan, J. Chen, X. Zhai, G. McKee, Q. Ren, X. Gong, C.T. Holcomb, W. Guo, L. Lao, J. Ferron, A. Hyatt, G. Staebler, W. Solomon, H. Du, Q. Zang, J. Huang, B. Wan, Phys. Plasmas 24 (5) (2017) 056114.
[6] Y. Sakamoto, Y. Kamada, S. Ide, T. Fujita, H. Shirai, T. Takizuka, Y. Koide, T. Fukuda, T. Oikawa, T. Suzuki, K. Shinohara, R. Yoshino, JT-60 Team, Nucl. Fusion 41 (7) (2001) 865–872.
[7] P.C. de Vries, E. Joffrin, M. Brix, C.D. Challis, K. Crombé, B. Esposito, N.C. Hawkes, C. Giroud, J. Hobirk, J. Lönnroth, P. Mantica, D. Strintzi, T. Tala, I. Voitsekhovitch, Nucl. Fusion 49 (7) (2009) 075007.
[8] L. Guazzotto, R. Betti, J. Manickam, S. Kaye, Phys. Plasmas 11 (2) (2004) 604–614.
[9] Y. Shi, G. Xu, F. Wang, M. Wang, J. Fu, Y. Li, W. Zhang, W. Zhang, J. Chang, B. Lv, J. Qian, J. Shan, F. Liu, S. Ding, B. Wan, S.G. Lee, M. Bitter, K. Hill, Phys. Rev. Lett. 106 (2011) 235001.
[10] C.C. Hegna, Phys. Plasmas 23 (5) (2016) 052514.
[11] S. Wang, Z.-W. Ma, Phys. Plasmas 22 (12) (2015) 122504.
[12] N. Aiba, S. Tokuda, M. Furukawa, P.B. Snyder, M.-S. Chu, Comput. Phys. Comm. 180 (8) (2009) 1282–1304.
[13] X.-T. Yan, P. Zhu, Y.-W. Sun, Phys. Plasmas 24 (8) (2017) 082510.

[14] R.J. La Haye, R.J. Buttery, Phys. Plasmas 16 (2) (2009) 022107.
[15] R.J. Buttery, R.J. La Haye, P. Gohil, G.L. Jackson, H. Reimerdes, E.J. Strait, the DIII-D Team, Phys. Plasmas 15 (5) (2008) 056115.
[16] K.P. Wessen, M. Persson, J. Plasma Phys. 45 (2) (1991) 267–283, 004.
[17] R.J. La Haye, C.C. Petty, P.A. Politzer, the DIII-D Team, Nucl. Fusion 51 (5) (2011) 053013.
[18] A. Sen, D. Chandra, P. Kaw, Nucl. Fusion 53 (5) (2013) 053006.
[19] R.J. La Haye, D.P. Brennan, R.J. Buttery, S.P. Gerhardt, Phys. Plasmas 17 (5) (2010) 056110.
[20] S.-K. Cheng, P. Zhu, D. Banerjee, Phys. Plasmas 24 (9) (2017) 092510.
[21] T.-Y. Xia, X.-Q. Xu, P.-W. Xi, Nucl. Fusion 53 (7) (2013) 073009.
[22] M.E. Fenstermacher, X.-Q. Xu, I. Joseph, M.J. Lanctot, C.J. Lasnier, W.H. Meyer, B. Tobias, L. Zeng, A.W. Leonard, T.H. Osborne, J. Nucl. Mater. 438 (Supplement) (2013) S346–S350, Proceedings of the 20th International Conference on Plasma-Surface Interactions in Controlled Fusion Devices.
[23] M.S. Chu, J.M. Greene, T.H. Jensen, R.L. Miller, A. Bondeson, R.W. Johnson, M.E. Mauel, Phys. Plasmas 2 (6) (1995) 2236–2241.
[24] D.J. Ward, A. Bondeson, Phys. Plasmas 2 (5) (1995) 1570–1580.
[25] S.P. Gerhardt, D.P. Brennan, R. Buttery, R.J. La Haye, S. Sabbagh, E. Strait, M. Bell, R. Bell, E. Fredrickson, D. Gates, B. LeBlanc, J. Menard, D. Stutman, K. Tritz, H. Yuh, Nucl. Fusion 49 (3) (2009) 032003.
[26] R. Betti, Phys. Plasmas 5 (10) (1998) 3615–3631.
[27] S.-B. Zheng, A.J. Wootton, Emilia R. Solano, Phys. Plasmas 3 (3) (1996) 1176–1178.
[28] C.V. Atanasiu, S. Günter, K. Lackner, I.G. Miron, Phys. Plasmas 11 (7) (2004) 3510–3518.
[29] L. Guazzotto, J.P. Freidberg, Phys. Plasmas 14 (11) (2007) 112508.
[30] P.J. Mc Carthy, Phys. Plasmas 6 (9) (1999) 3554–3560.
[31] S. Šesnić, D. Poljak, E. Slišković, 2014 22nd International Conference on Software, Telecommunications and Computer Networks (SoftCOM), IEEE, 2014, pp. 24–27.
[32] P.B. Parks, M.J. Schaffer, Phys. Plasmas 10 (5) (2003) 1411–1423.
[33] H.L. Berk, J.H. Hammer, H. Weitzner, Phys. Fluids 24 (9) (1981) 1758–1759.
[34] S.-J. Wang, Phys. Rev. Lett. 93 (2004) 155007.
[35] A.J. Cerfon, J.P. Freidberg, Phys. Plasmas 17 (3) (2010) 032502.
[36] F. Crisanti, J. Plasma Phys. 85 (2) (2019) 905850210.
[37] J.L. Johnson, H.E. Dalhed, J.M. Greene, R.C. Grimm, Y.Y. Hsieh, S.C. Jardin, J. Manickam, M. Okabayashi, R.G. Storer, A.M.M. Todd, D.E. Voss, K.E. Weimer, J. Comput. Phys. 32 (2) (1979) 212–234.
[38] K.M. Ling, S.C. Jardin, J. Comput. Phys. 58 (3) (1985) 300–335.
[39] L.L. Lao, H. St. John, R.D. Stambaugh, A.G. Kellman, W. Pfeiffer, Nucl. Fusion 25 (11) (1985) 1611–1622.
[40] J. Blum, J. Le Foll, B. Thooris, Comput. Phys. Comm. 24 (3) (1981) 235–254.
[41] R. Gruber, R. Iacono, F. Troyon, J. Comput. Phys. 73 (1) (1987) 168–182.
[42] H. Lütjens, A. Bondeson, A. Roy, Comput. Phys. Comm. 69 (2) (1992) 287–298.
[43] L.E. Zakharov, A. Pletzer, Phys. Plasmas 6 (12) (1999) 4693–4704.
[44] E.C. Howell, C.R. Sovinec, Comput. Phys. Comm. 185 (5) (2014) 1415–1421.
[45] S. Semenzato, R. Gruber, H.P. Zehrfeld, Comput. Phys. Rep. 1 (7) (1984) 389–425.
[46] A.J.C. Beliën, M.A. Botchev, J.P. Goedbloed, B. van der Holst, R. Keppens, J. Comput. Phys. 182 (1) (2002) 91–117.
[47] C.R. Sovinec, A.H. Glasser, T.A. Gianakon, D.C. Barnes, R.A. Nebel, S.E. Kruger, D.D. Schnack, S.J. Plimpton, A. Tarditi, M.-S. Chu, J. Comput. Phys. 195 (1) (2004) 355–386.
[48] E.K. Maschke, H. Perrin, Plasma Phys. 22 (6) (1980) 579.
[49] M. Furukama, Y. Akamura, S. Amaguchi, M. Wakatani, J. Plasma Fusion Res. 76 (9) (2000) 937–948.
[50] E. Hameiri, Phys. Fluids 26 (1) (1983) 230–237.
[51] L.S. Solov'ev, Sov. Phys.—JETP 26 (1968).
[52] M.-S. Chu, Y.-M. Hu, W.-F. Guo, Plasma Sci. Technol. 20 (3) (2018) 035101.
[53] J.P. Boyd, Chebyshev and Fourier Spectral Methods, second edition ed., DOVER Publications, Inc, 2000.

Please cite this article as: H. Li and P. Zhu, Solving the Grad–Shafranov equation using spectral elements for tokamak equilibrium with toroidal rotation, Computer Physics Communications (2020) 107264, https://doi.org/10.1016/j.cpc.2020.107264.